



**HAL**  
open science

## Cytochrome c oxidase deficiency detection in human fibroblasts using scanning electrochemical microscopy

Shubhneet Thind, Dhésmon Lima, Evan Booy, Dao Trinh, Sean Mckenna,  
Sabine Kuss

► **To cite this version:**

Shubhneet Thind, Dhésmon Lima, Evan Booy, Dao Trinh, Sean Mckenna, et al.. Cytochrome c oxidase deficiency detection in human fibroblasts using scanning electrochemical microscopy. Proceedings of the National Academy of Sciences of the United States of America, 2023, 121 (1), 10.1073/pnas.2310288120 . hal-04457632

**HAL Id: hal-04457632**

**<https://hal.science/hal-04457632>**

Submitted on 14 Feb 2024

**HAL** is a multi-disciplinary open access archive for the deposit and dissemination of scientific research documents, whether they are published or not. The documents may come from teaching and research institutions in France or abroad, or from public or private research centers.

L'archive ouverte pluridisciplinaire **HAL**, est destinée au dépôt et à la diffusion de documents scientifiques de niveau recherche, publiés ou non, émanant des établissements d'enseignement et de recherche français ou étrangers, des laboratoires publics ou privés.

## Cytochrome *c* oxidase deficiency detection in human fibroblasts using scanning electrochemical microscopy

Shubhneet Thind<sup>a</sup>, Dhésmon Lima<sup>a</sup>, Evan Booy<sup>b</sup>, Dao Trinh<sup>c</sup>, Sean McKenna<sup>b</sup> and Sabine Kuss<sup>a,\*</sup>

<sup>a</sup>Laboratory for Bioanalytics and Electrochemical Sensing, Department of Chemistry, University of Manitoba, 144 Dysart Road, R3T 2N2, Winnipeg, Manitoba, Canada

<sup>b</sup>Department of Chemistry, University of Manitoba, 144 Dysart Road, R3T 2N2, Winnipeg, Manitoba, Canada

<sup>c</sup>Laboratoire des Sciences de l'Ingénieur pour l'Environnement (LaSIE) UMR CNRS 7356, Université de La Rochelle, Pôle Sciences et Technologie, Avenue Michel Crépeau, 17042, La Rochelle, Cedex 1, France

\*Corresponding author: Dr. Sabine Kuss

**Email:** [sabine.kuss@umanitoba.ca](mailto:sabine.kuss@umanitoba.ca)

**Author Contributions:** S. T. performed all experiments, data analysis and wrote the manuscript. D. L. wrote and reviewed the manuscript. E. B. performed experiments and assisted during data analysis. D. T. performed numerical modeling analysis. S. K. designed and supervised the research, obtained funding, and wrote and revised the manuscript.

**Competing Interest Statement:** The authors declare that they have no known competing financial interests or personal relationships that could have appeared to influence the work reported in this paper.

**Classification:** Major: Physical Sciences; Minor: Applied Physical Sciences

**Keywords:** cytochrome *c* oxidase deficiency; scanning electrochemical microscopy; single-cell analysis; electrochemistry

### This PDF file includes:

Main Text  
Figures 1 to 5

## **Abstract**

Cytochrome C Oxidase Deficiency (COXD) is an inherited disorder characterized by the absence or mutation in the genes encoding for the cytochrome c oxidase protein (COX). COX deficiency results in severe muscle weakness, heart, liver, and kidney disorders, as well as brain damage in infants and adolescents, leading to death in many cases. With no cure for this disorder, finding an efficient, inexpensive, and early means of diagnosis is essential to minimize symptoms and long-term disabilities. Furthermore, muscle biopsy, the traditional detection method, is invasive, expensive, and time-consuming. This study demonstrates the applicability of scanning electrochemical microscopy to quantify COX activity in living human fibroblast cells. Taking advantage of the interaction between the redox mediator N,N,N',N'-tetramethyl-*para*-phenylene-diamine, and COX, the enzymatic activity was successfully quantified by monitoring current changes using a platinum microelectrode and determining the apparent heterogeneous rate constant  $k_0$  using numerical modeling. This study provides a foundation for developing a new diagnostic method for detecting COXD in infants, which has the potential to increase treatment effectiveness and improve the quality of life of affected individuals.

## **Significance Statement**

Cytochrome C Oxidase deficiency (COXD) is an incurable mitochondrial disease, but symptoms in young infants can be managed if an early diagnosis is made, improving the quality of life of affected individuals. Currently, this disorder is diagnosed through muscle biopsies which are invasive, expensive, and time-consuming, leading to a delay in diagnosis. Our study proposes the quantification of cytochrome c oxidase (COX) activity in living fibroblasts using Scanning Electrochemical Microscopy (SECM) as an indicator for the quick, non-invasive, and accurate diagnosis of COXD. Our results will form the basis for the future development of a biosensor for the routine detection of COXD in tissue samples, therefore benefiting healthcare systems and newborns around the world.

## **Main Text**

### **Introduction**

Cytochrome c oxidase (COX), also known as Complex IV, is a multimeric protein comprised of fourteen subunits that act as the terminal electron acceptor of the electron transport chain, which is responsible for coupling oxidative phosphorylation with ATP production (1, 2). Found in the inner membrane of the mammalian mitochondria (2), three of the subunits of this transmembrane protein are encoded by mitochondrial DNA while

the others are encoded by nuclear DNA (3). Mutations in mitochondrial or nuclear genes encoding COX lead to the incorrect assembly of COX, resulting in functional defects which cause a rare heterogenous disorder called cytochrome c oxidase deficiency (COXD) (4). This disorder dramatically affects vital organs such as the heart, brain, liver, and skeletal muscles, causing a range of degenerative diseases, from lethal infantile myopathy to Leigh Syndrome and Hepatic Encephalopathy (4–6). Being the most prevalent among all mitochondrial disorders (30% of the cases) (7, 8), which affect 1 in 5000 people worldwide (9), COXD is often fatal in childhood, with only a few individuals surviving adolescence (4, 10). Mutations in thirty possible nuclear and mitochondrial genes are known to cause COXD (4), which includes alterations in the *SCO1* nuclear-encoded gene. *SCO1* encodes the *SCO1* metallochaperone protein (11, 12), which mediates copper transport from subunit COX17 to COX2, allowing the assembly of the CuA copper site in COX and ultimately enabling the proper biosynthesis of the protein (3, 11). Therefore, mutations in *SCO1* indirectly impair the proper assembly of COX, leading to the biosynthesis of non-functional COX molecules. COXD caused by *SCO1* mutation results in clinical phenotypes such as hepatic failure (13), fatal encephalopathy (4), and ketoacidosis (7).

Currently, COXD is diagnosed by collecting skin and muscle biopsy samples from patients which are subject to a variety of enzyme assays and histochemical methods including spectrophotometric, immunofluorescent, and cytochrome c oxidase/succinate dehydrogenase double-labeling (COX/SDH) assays (14–18). These methods present several drawbacks. For instance, COX/SDH is often limited by its inability to detect COXD at low levels due to this method's dependence on staining (19). Immunofluorescence-based methods require expensive antibodies to detect COX activity, which significantly increases the cost of the technique (17, 20). Additionally, these assays are labor-intensive, time-consuming, and often require invasive muscle biopsies from young patients (17, 19, 21), as non-invasive means of COX diagnosis are currently non-existent (15). The development of alternative sensitive methods that are capable of diagnosing COXD inexpensively, quickly, and non-invasively, is therefore crucial.

Electrochemical methods have revealed an outstanding potential to be used as diagnostic assays to detect many disease biomarkers. Specifically, scanning electrochemical microscopy (SECM) stands out as an innovative technique that can detect trace levels of biomolecules with high spatial and temporal resolution. During SECM, while recording its lateral tip position, a microelectrode is scanned across an underlying surface

monitoring an electrochemical current. Unlike other scanning probe techniques, SECM not only reveals the topography of samples in a solution but also enables the detection and visualization of local variations in the electrochemical reactivity of the investigated sample. The high sensitivity of this method, its non-invasive nature, and the micrometric dimensions of the sensor make SECM a particularly attractive technique to study biological samples, such as living cells and tissues (22–24). In fact, several promising biological applications of SECM have been described, including the study and detection of human cancer (25–27), and bacterial metabolism (28–30). The exceptional features of SECM make it an ideal tool to detect new cellular biomarkers and cell metabolites at the single-cell level (31, 32) that can later be transferred onto portable, cost-efficient, and user-friendly biosensing platforms.

In this study, we propose a sensitive electroanalytical method based on SECM to quantify COX activity in living primary fibroblasts, which are known for being a model cell line used to study mitochondrial disorders associated with COX (33). Our detection approach uses the redox mediator N,N,N',N'-tetramethyl-*para*-phenylene-diamine (TMPD). TMPD is commonly used as the substrate in the oxidase test to determine the presence of cytochrome *c* oxidases in bacteria (34, 35), and has been previously employed to quantify bacterial cytochrome *c* oxidase activity using electrochemistry (36). Herein, SECM measures fibroblasts' ability to oxidize TMPD to TMPD<sup>•+</sup>, which is mediated by COX. The redox species diffuse through the mitochondrial outer membrane and cross the lipid cell bilayer to reach the microelectrode, where it is reduced. The generated current response is a convoluted signal that is influenced by the cell's reactivity, but also by the cell's topography (37). To decouple the effect of topography and reactivity on the detected current signal, a numerical modeling approach described previously is employed (26, 38). This methodology enables the extraction of the apparent heterogeneous rate constant and, thereby quantifying COX activity in living fibroblasts. This is the first report on an electrochemical method devoted to investigating COXD, and the presented results will serve as a foundation for the future development of a portable biosensor for COXD diagnosis.

## **Results and Discussion**

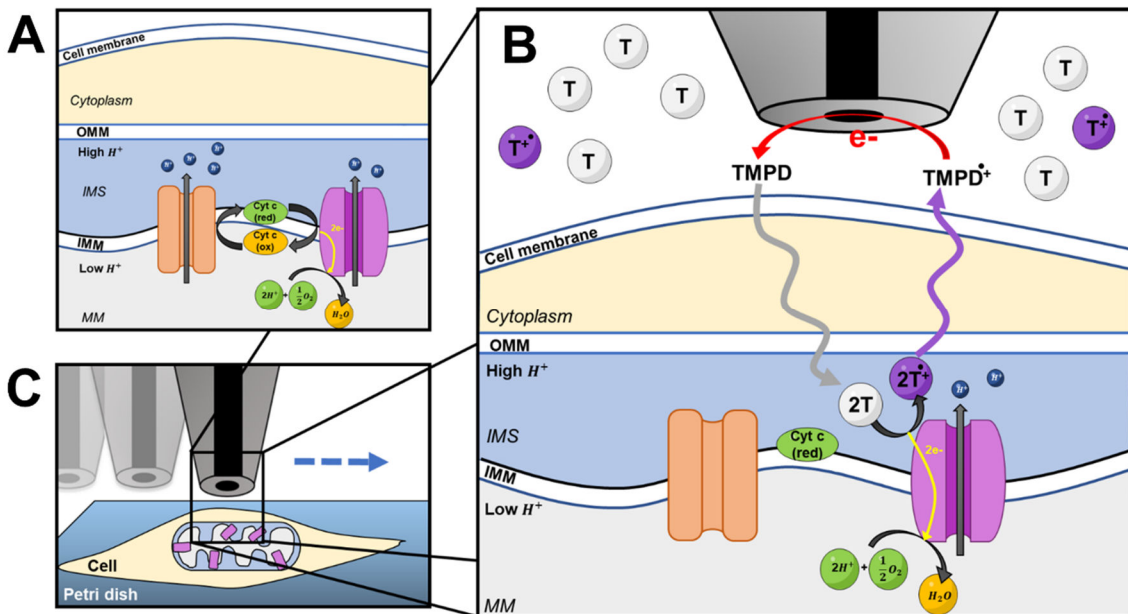
### *COX redox mechanism and TMPD electrochemistry*

As seen in Scheme 1A, under normal aerobic conditions, COX catalyzes the electron transfer from reduced cytochrome *c* to molecular oxygen, resulting in water and oxidized cytochrome *c*, while transporting one proton per electron from the matrix to the intermembranous space (2). Simultaneously, cytochrome *c* oxidoreductase or complex III (CRE) pumps two protons per electron while catalyzing electron transfer from ubiquinol (QH<sub>2</sub>) to oxidized cytochrome *c*, restoring cytochrome *c* to its reduced form. Cytochrome *c* can only transfer one electron at a time; hence, to produce one water molecule, cytochrome *c* must undergo reduction twice (2).

To enable the electrochemical detection of COX activity using SECM, we used TMPD as the redox mediator due to its well-known interaction with the protein (34–36). In the presence of TMPD concentrations higher than 0.4 mM, electron transfer reactions can occur directly from TMPD to COX, without the involvement of cytochrome *c* (39, 40). Scheme 1B proposes the cellular uptake of the membrane-permeable redox mediator TMPD (39). TMPD crosses the outer cell membrane barrier, as well as the mitochondrial outer membrane, interacting with COX located in the inner mitochondrial membrane. TMPD undergoes oxidization to TMPD<sup>+</sup>, transferring one electron to COX to reduce oxygen to produce water (41). Just as in the case of cytochrome *c*, two TMPD molecules are required to produce one water molecule. COX can transport one proton per electron into the intermembranous space, allowing ATP synthesis to continue through the ATP synthase. Once oxidized, TMPD<sup>+</sup> passes through the outer mitochondrial membrane and the cell plasma membrane to interact with the surface of the microelectrode as it passes over the cell, as seen in Scheme 1C. A reduction potential, applied at the electrode

reduces  $\text{TMPD}^{2+}$  back to  $\text{TMPD}$ , creating a feedback loop, which produces an increase in electrochemical current during SECM imaging.

To understand  $\text{TMPD}$ 's role as a redox mediator for single-cell SECM studies, it was electrochemically characterized using cyclic voltammetry.  $\text{TMPD}$  undergoes two electron transfer steps, generating  $\text{TMPD}^{+}$  first, and  $\text{TMPD}^{2+}$  in the second electron transfer step (42). As shown in Figure 1A,  $\text{TMPD}$  oxidizes at +200 mV to produce  $\text{TMPD}^{+}$  and is subsequently oxidized to  $\text{TMPD}^{2+}$  at +600 mV. Reduction potentials are observed at +200 mV and -200 mV. The effect of electrolyte composition was studied in DMEM cell media, in the presence and the absence of FBS, and 0.1 M KCl (Figure S1). Although similar voltammetric profiles were observed for  $\text{TMPD}$  in DMEM media with and without FBS (Figure S1), all SECM experiments were performed in the absence of serum, because of potential electrode fouling over time (43). To avoid the formation of the unstable  $\text{TMPD}^{2+}$ , SECM measurements on living cells were performed by applying a potential at the microelectrode that corresponds to the first electron transfer step ( $\text{TMPD}$  to  $\text{TMPD}^{+}$  and *vice versa*).



**Scheme 1.** Schematic representation of cellular and electrochemical reactions. (A) COX (violet) and cytochrome c reductase (orange) complexes under normal aerobic conditions in a mammalian cell. (B) SECM measurements at 12  $\mu\text{m}$  above the surface of a single fibroblast cell in 1 mM  $\text{TMPD}$  in feedback mode (C). Proposed mechanism of Complex IV under  $\text{TMPD}$  concentration > 0.4 mM,  $\text{TMPD}$  (T),  $\text{TMPD}^{+}$  ( $\text{T}^{+}$ ), OMM: Outer mitochondrial membrane, IMS: Inter-membrane space, IMM: Inner mitochondrial membrane, MM: Mitochondrial matrix.

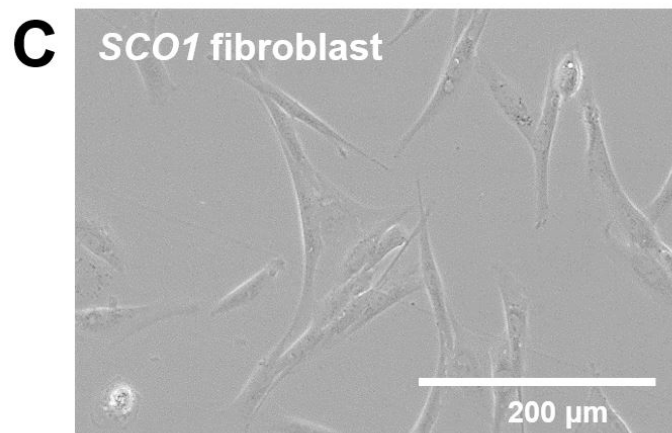
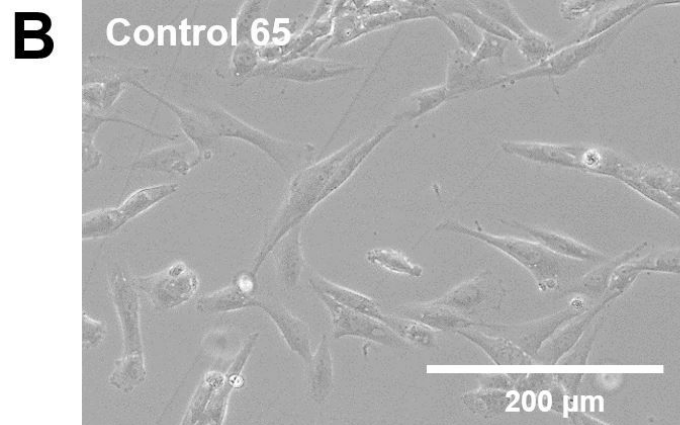
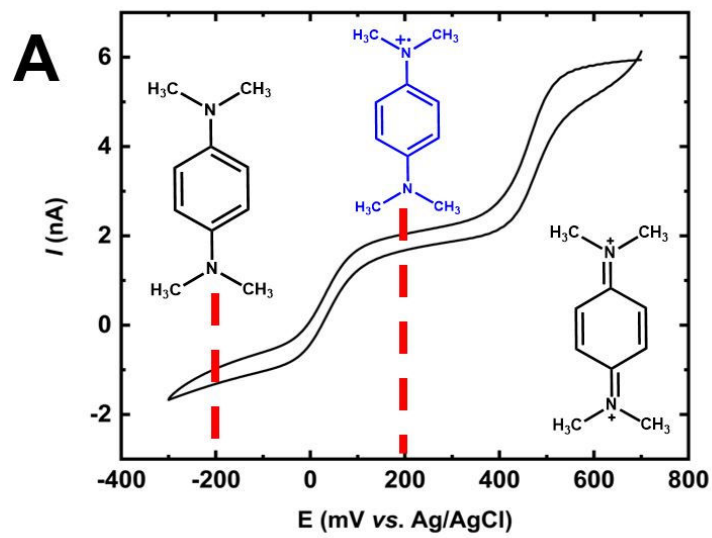


**Fig. 1.** TMPD electrochemistry and cell morphology. (A) Voltametric profile of N,N,N',N'-tetramethyl-para-phenylenediamine (TMPD) on a bare 25- $\mu\text{m}$  platinum microelectrode. Reduction and oxidation potentials of TMPD are shown by red dotted lines (respectively). (B) Optical micrographs of Control and (C) SCO1 fibroblast lines.

## Electrochemical monitoring of TMPD interaction with living fibroblasts

The two fibroblast cell lines used in this work included a control cell line (Control 65) of healthy fibroblasts, capable of expressing a fully assembled and functional COX enzyme. SCO1 cells carry the *SCO1* gene mutation that impairs the proper biosynthesis of COX (3, 11). Both cell types present a similar morphology, characterized by an elongated shape with a fibrous aspect (Figures 1B and C). To validate the cell lines of choice, expression levels of fully assembled COX and SCO1 proteins in the Control and SCO1 cell lines were quantified by Western blot analysis. The SDS-PAGE result displayed in Figure 2A confirms the reduced level of SCO1 protein (29 kDa) in SCO1 cells. VDAC1 (35 kDa) was used as a loading control and was detected equally in both cell lines. Accordingly, the BN-PAGE results (Figure 2B) show that cells carrying the *SCO1* mutation present reduced levels of fully assembled COX due to decreased levels of SCO1 protein (9). Complex I was used as a loading control and was detected equally in both fibroblast lines. The decreased levels of SCO1 and COX proteins in SCO1 cells, therefore, validate SCO1 as a COXD cell line. Differential electrochemical signals are expected for COX activity in Control cells compared to SCO1-deficient fibroblast cells.

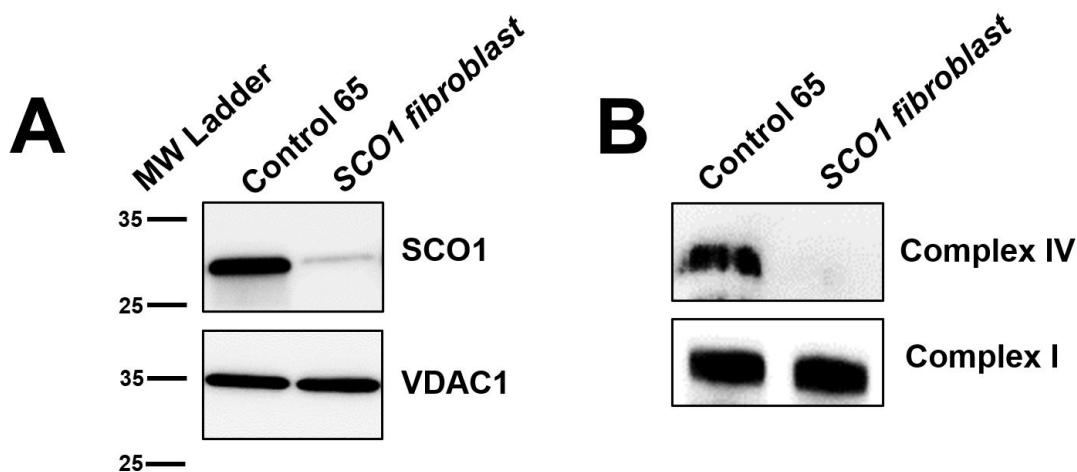


**Fig. 2.** Western blot results of mitoplasts isolated from Control and SCO1 fibroblast cells. (A) Fibroblasts fractionated by SDS-PAGE and blot were subject to antibodies against SCO1. VDAC1 was used as a loading control. Molecular weight (MW) protein ladder is indicated on the left. (B) Fibroblasts fractionated by 1D BN-PAGE and blot were subject to antibodies against complex IV. Complex I was used as a loading control.

Prior to SECM measurements, cells were exposed to DMEM basic media (no FBS) in the presence of 1 mM TMPD for 15 min. Cell viability was not affected by TMPD exposure according to a Trypan Blue exclusion cell viability assay in the literature, where it has been reported previously that cell exposure to TMPD for 15 min does not affect viability (44). However, the absence of FBS in the cell culture media is known to affect both cell viability and morphology (43). By conducting a cell viability study over 90 min, we were able to confirm that the viability and morphology of Control and SCO1 fibroblast lines remained unaffected for the first 60 min (Figure S2), and no external signs of stress were observed through the SECM-integrated optical microscope. This ensures that fibroblasts remained viable during all SECM line scans.

Three-dimensional SECM images (Figure 3) of single Control and SCO1 fibroblasts show a differential current behavior between the two cell lines, qualitatively. In this representative example of an experimental data set, larger current signals from a Control cell (Figures 3C and D) can be seen compared to the current obtained from a SCO1 cell (Figures 3A and B). Three-dimensional images were obtained in TMPD at 50  $\mu\text{m s}^{-1}$  scan velocity, using a microelectrode biased at the potentials of +200 mV (oxidations of TMPD) or -200 mV (reduction of TMPD). It should be noted that a solution of TMPD prepared in the presence of oxygen naturally presents a ratio of 3:1 of reduced and oxidized TMPD (36), respectively. When a reduction potential of -200 mV is applied, the electrode detects the ability of the living cells to oxidize TMPD to  $\text{TMPD}^{+\bullet}$ , which is reduced back to TMPD at the microelectrode (Scheme 1). During SECM imaging of living cells, the measured signal is always a convolution of topographical contributions and reactivity-related signals (26, 38). Topographical contributions result in a decrease in current, because of the hindered diffusion of the redox active species towards the electrode due to the topography of the cell. Reactivity describes the regeneration of the redox mediator by the living cell. As shown in Figures 3A and C, as the microelectrode passes over the cells, a clear increase in the electrochemical current signal was observed. In this case, the reactivity of the cells is able to overcompensate for the topographical contributions, resulting in an overall increase in current when the electrode passes the cell located on the petri dish. Similarly, when an oxidation potential of +200 mV is employed (Figures 3B and D), the electrode detects the ability of the living cells to reduce  $\text{TMPD}^{+\bullet}$  to TMPD, which is then oxidized to  $\text{TMPD}^{+\bullet}$  at the microelectrode. In this case, the reactivity of the cells is not able to overcompensate for the contributions from the cell

topography, resulting in an overall decrease in current when the electrode scans across the living cells (Figure 3B and D). Interestingly, depending on the applied potential at the microelectrode, SECM is able to monitor the activity of both cytochrome oxidase and reductase.

However, the qualitative assessment of currents is inaccurate and can be misleading as cells of different shapes and sizes will have differential contributions to the measured electrochemical current from topography and reactivity. Numerical modeling is an effective and accurate tool to decouple topography from reactivity and extract an apparent heterogeneous rate constant  $k_0$ , which indicates the cell's ability to regenerate a redox mediator in solution (26, 38, 45).

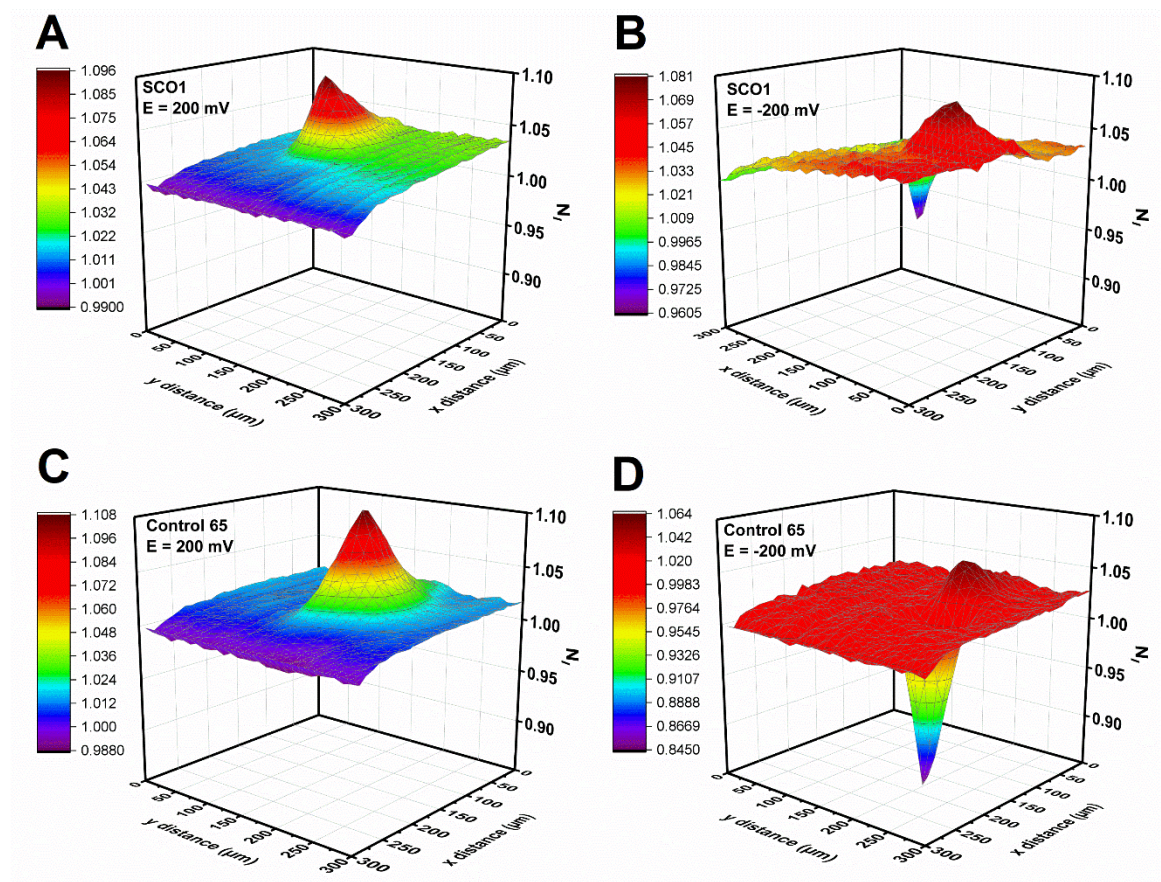


**Fig. 3.** SECM 3D imaging of single living fibroblasts at  $50 \mu\text{m s}^{-1}$ . Microelectrode polarized at +200 mV and -200 mV to scan Control (A and B) and SCO1 fibroblasts (C and D).

Figure 4 demonstrates SECM line scans in TMPD across Control and SCO1 cells at varying scan rates (10 to 100  $\mu\text{m s}^{-1}$ ). It is evident that, as the scan velocity is increased, the current measured at the microelectrode also increases because of greater mass transport caused by forced convection (38). Thereby, electrochemical currents that originate from contributions by topography are more susceptible to scan velocity changes, than contributions from reactivity. This forms the basis of the previously reported numerical model, capable of decoupling topography from reactivity (26).

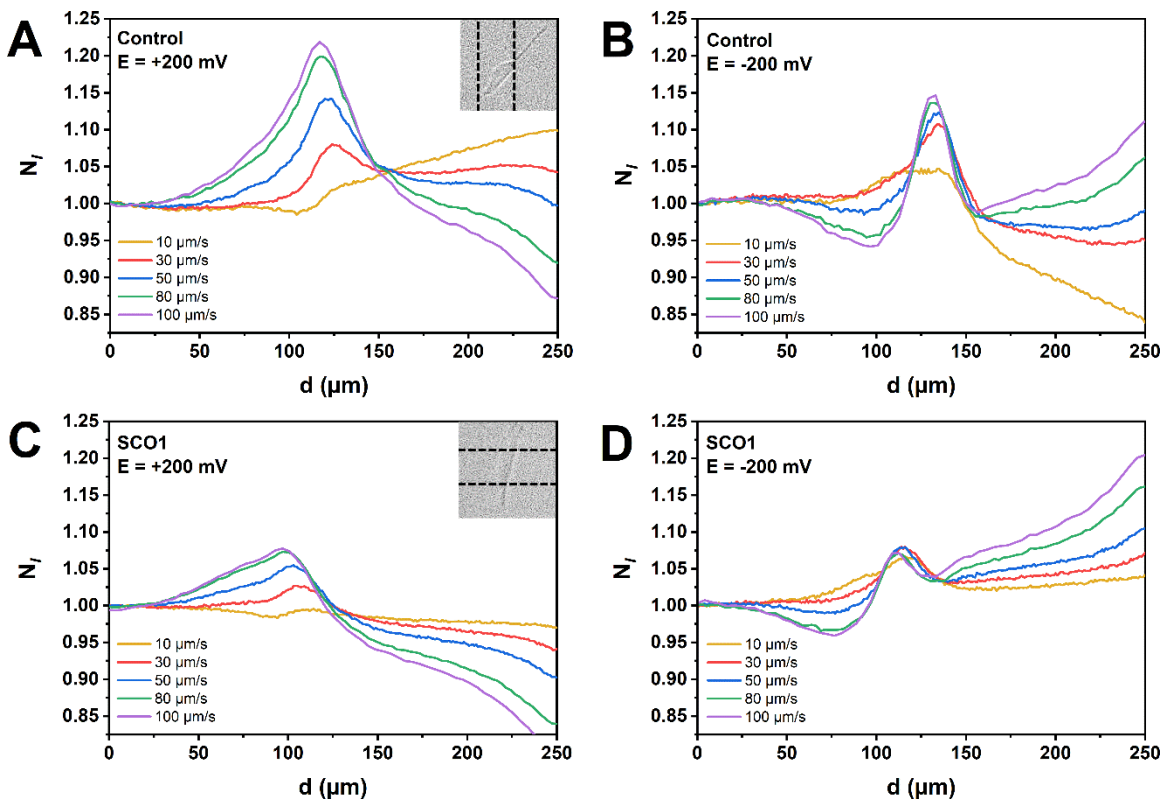


**Fig. 4.** SECM line scans across fibroblast cells. Imaging of single living Control (A and B) and SCO1 (C and D) fibroblasts in basic DMEM media containing 1 mM TMPD, with scan velocities ranging from 10 to 100  $\mu\text{m s}^{-1}$  and the microelectrode biased at +200 V (A and C) and -200 V (B and D). Normalized currents shown (current divided by current in bulk solution). Insets show optical micrographs of the studied cells and the electrode edge path during line scan acquisition is represented by the black dashed lines.

#### *Extraction of the apparent heterogeneous rate constant ( $k_0$ )*

Using numerical modeling, TMPD oxidation and TMPD<sup>+</sup> reduction occurring at the microelectrode after interaction with COX and cytochrome c reductase (CRE) in living fibroblasts can be utilized to extract the apparent heterogeneous rate constant ( $k_0$ ), representing the biological cell kinetics. This mathematical approach was described in

detail in previous work (38, 45), and is based on the extraction of a substrate's kinetic rate from electrochemical data obtained using SECM constant height imaging at slow scan velocities ( $<100 \mu\text{m s}^{-1}$ ). The numerical COMSOL model considers experimental parameters such as the microelectrode size, steady state current, scan velocity, diffusion parameters of redox species, as well as cellular features, including the cell's shape and size to quantify the redox environment of a cell. This mathematical approach fits the theoretical results from the substrate kinetic rates varying from  $10^{-8} \text{ m s}^{-1}$  to  $10^{-1} \text{ m s}^{-1}$  to the normalized current detected at the microelectrode as the function of scan velocities. Because the microelectrode current depends on the scan velocity of the tip, the diffusion coefficient, and the tip-to-sample distance, the kinetic rates can be extracted from the normalized shear Peclet number (Ps) (38).

A visualization of the electrode and fluid movement within the simulation is presented in Figure S3. When a microelectrode passes a living cell, the cell-surrounding fluid is forced to pass in between the electrode tip and the body of the cell. Because of the limited amount of space for the fluid to pass, the concentration of the redox species in between the cell is temporarily increased. The height of a cell thereby affects the measured current more than the reactivity of the cell, which remains constant. The faster the scan velocity, the more fluid is pushed between the microelectrode and the cell. By simulating the scanning profiles for several scan velocities, an average kinetic rate  $k_0$  can be extracted. Figure 5 shows the normalized tip current as a function of Ps for the Control and SCO1 fibroblasts (Figures 5A and 5C, respectively). For both COX and CRE activity, the SCO1 values are lower than the Control values, confirming slower kinetic rates in the SCO1 fibroblasts. These kinetic rates can be determined by fitting the normalized current on the simulation curve for both COX activity (Figure 5B) and CRE activity (Figure 5D). The average estimated  $k_0$  value obtained for COX activity from Control and SCO1 cells ( $n = 4$  for each cell line) was  $3.49 \times 10^{-5} \text{ m s}^{-1}$  and  $2.10 \times 10^{-5} \text{ m s}^{-1}$ , respectively. These results indicate a statistically significantly slower COX kinetic rate for the COX-deficient cell line. Similarly, the average  $k_0$  value for CRE activity was determined to be equal to  $4.16 \times 10^{-5} \text{ m s}^{-1}$  and  $2.35 \times 10^{-5} \text{ m s}^{-1}$  for Control and SCO1 fibroblasts ( $n = 4$  for each cell line), respectively.

Two-sample two-tailed t-tests performed with the results showed that the difference in the average  $k_0$  values for COX activity between Control and SCO1 fibroblasts is statistically significant ( $P < 0.10$ ), whereas it was found to be non-significant when the

CRE activity was analyzed ( $P > 0.10$ ). These results are in clear agreement with the phenotype of the cells analyzed in this study. The mutation in the *SCO1* gene in *SCO1* fibroblasts affects the biosynthesis of COX, with no direct effect on the expression of the CRE enzyme. However, the observable trend of reduced activity of CRE in *SCO1* cells is not surprising as the activities of the enzyme complexes in the electron transport chain are intrinsically connected (46, 47). The statistically significant difference in  $k_0$  between Control and *SCO1* cells with regards to COX activity is, therefore, a robust indicator that cellular phenotypes of COXD can be accurately and quantitatively monitored using SECM.

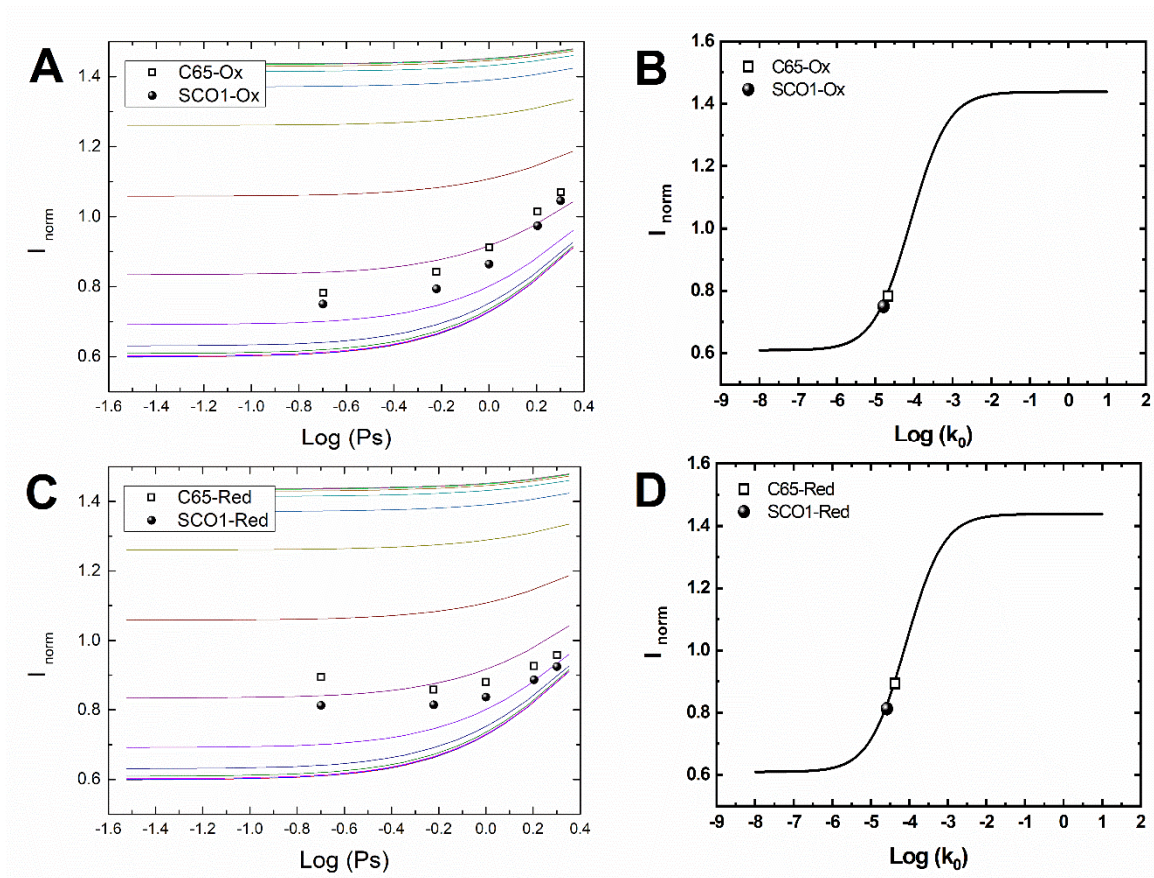


**Fig. 5.** Summary of the numerical modeling results for the analysis of Control and *SCO1* fibroblasts using SECM. (A, B) COX activity. (C-D) CRE activity. (A, C) The colored lines represent the simulated normalized peak currents for several substrate and sample kinetics ranging from  $10^{-8}$  to  $10^1$   $\text{m s}^{-1}$ . The current signal for Control (square) is higher than the one for *SCO1* fibroblast (circle). (B, D) The normalized current is taken at low  $P_s$  ( $<1$ ) as a function of kinetic  $k_0$ .

## Conclusions

In this study, we present SECM as a promising and effective method to detect and quantify COX activity in living fibroblasts. The presented electroanalytical approach was based on quantifying current variations resulting from the interaction of the redox mediator TMPD with living cells, followed by extracting an apparent heterogeneous rate constant for the turnover of TMPD/TMPD<sup>+</sup> by single cells using numerical modeling. The study of the cell reaction kinetics allowed us to successfully decouple the effects of cell reactivity and cell topography on the overall bioelectrochemical response, hence giving insight into the differential COX activity between Control and SCO1 deficient cells. TMPD/TMPD<sup>+</sup> regeneration was found to be considerably slower in the SCO1 cell line compared to healthy control cells, making this SECM approach a reliable method for COX activity detection in human cells. The insight generated in this proof-of-concept study can be further employed in the development of an electrochemical biosensor for COXD clinical diagnostics. Moreover, our study confirms the ability of SECM to identify new biomarkers for diseases and pave the path for the development of new biomedical detection assays.

## **Material and Methods**

All chemicals were purchased from Sigma-Aldrich (Canada), and all media and materials for cell culture and related assays were purchased from Thermo-Fisher Scientific (USA) unless otherwise stated.

### *Cell Culture and sample preparation for SECM analysis*

Control and SCO1 skin fibroblast cell lines were provided by Dr. Eric Shoubridge (McGill University, Canada). These two primary immortalized cell lines were cultured in Dulbecco's Modified Eagle's medium (DMEM) supplemented with 10% heat-inactivated fetal bovine serum (FBS), in tissue culture flasks at 37 °C and 5% CO<sub>2</sub>. After reaching 80-90% confluency, cells were harvested. To this end, cells were washed with 0.0067 M phosphate-buffered saline (PBS, pH 7.0 at 37 °C) and detached from the surface of the flask using 0.05% trypsin-EDTA solution at 37 °C. For SECM analysis, around 40,000 cells

were seeded in 10 mm x 35 mm Petri dishes and incubated overnight under the conditions described above.

#### *Western blot assay*

Following procedures previously described (12, 48, 49), fully assembled COX was detected by subjecting mitoplasts from Control and SCO1 fibroblasts to blue native page gel electrophoresis (BN-PAGE). Mitoplasts were initially isolated using a mitochondrial isolation kit (89874, Thermo-Fisher Scientific). For BN-PAGE analysis, sedimented mitochondria were resuspended in 0.75 M aminocaproic acid and 50 mM Bis-Tris buffer at pH 7. 10% n-dodecyl-B-D-maltopyranoside was then added to the suspension and incubated on ice for 30 minutes. The mixture was centrifuged at 16,000 x g for 30 minutes before 5% Coomassie Brilliant Blue stain in 0.5 M aminocaproic acid was added to the supernatant. For first dimension separation, a 6-15% native polyacrylamide gradient gel was used. The blot was subjected to antibodies against COX (ab14744, Abcam, Cambridge, UK) and loading control complex I (ab110412, Abcam, Cambridge, UK). SDS-PAGE was performed as previously described by Booy et al. (50), to detect SCO1 protein in Control and SCO1 fibroblasts. This blot was subjected to antibodies against SCO1 (PA554460 Invitrogen, MA, USA) and loading control VDAC1 (MABN504 MilliporeSigma, MA, USA). HRP-conjugated goat anti-rabbit (12348) and HRP-conjugated goat anti-mouse (12349) antibodies (Millipore Sigma) were used for chemiluminescent detection. Proteins were visualized using a ChemiDoc System (Bio Rad, CA, USA).

#### *Cell viability assay*

To determine the viability of fibroblasts in the presence of TMPD, Trypan Blue Exclusion assays were conducted for Control and SCO1 cell lines. Cells were exposed to 1 mM TMPD in basic DMEM media (no FBS) for varying time intervals of 10, 30, 60, and 90 minutes. The medium was removed, cells were washed with PBS, and then harvested after treatment with trypsin. Subsequently, fibroblasts were incubated in the presence of Trypan Blue (1:1) at room temperature for 3 minutes (51). Percent cell viability was determined using a Countess 2 Automated Cell Counter (Thermo Scientific, USA).

### *SECM measurements*

All electrochemical experiments were performed using an EIProScan ELP3 system, with POTMASTER software (version V2 × 66) and an EIProScan Controller ESC 3 (HEKA Elektronik, Germany). A three-electrode setup consisting of an Ag/AgCl reference electrode, a 0.5 mm diameter platinum wire auxiliary electrode, and a 25 μm platinum microelectrode (RG = 2.8, HEKA Elektronik, Germany) was used. Prior to any measurement, the platinum microelectrode was polished using 0.05 μm alumina slurry (Buehler, USA) on an automated electrode polisher (LaboPol-20, Struers Inc., USA). The electrochemical behavior of TMPD in basic DMEM cell media (no FBS) was investigated using cyclic voltammetry, with measurements carried out at a potential scan rate of 100 mV s<sup>-1</sup>.

All SECM imaging measurements were carried out in feedback mode. TMPD (1 mM) was used as a redox mediator and was dissolved in basic DMEM media (no FBS). Prior to cell exposure, the TMPD solution was sterile-filtered using a 0.22 μm pore syringe filter (Millipore Sigma). Cells were incubated in the TMPD solution for 20 min at 37 °C before SECM data acquisition. Target fibroblasts were identified using an optical microscope located underneath the SECM stage. Prior to commencing line scans, a tip-to-substrate distance of 12 μm was achieved through a negative feedback approach curve over plastic in close proximity to a living cell of interest (38). All biological samples for this study were scanned at constant height with scan velocities ranging from 10 to 100 μm s<sup>-1</sup>. During SECM data collection, cell dimensions, and morphology were constantly monitored using the SECM-integrated optical microscope. To ensure cell viability, SECM measurements were collected in under 30 minutes in the presence of the TMPD redox mediator.

### *Statistical analysis*

All experiments were performed in quadruples (unless stated otherwise). Two-sample t-Test was used to determine whether the difference in mean apparent heterogeneous rate constants between Control 65 and SCO1 fibroblast cells differed significantly. For both COX and CRE activity, a  $P < 0.10$  was considered statistically significant. Statistical analyses were performed using Origin 2019.

## Acknowledgments

The authors SK, ST, and DL thank Drs. Christian Heinemann and Frank Wang from HEKA Elektronik GmbH for the technical support on the SPECM instrument and software integrations. The authors thank Dr. Eric Shoubridge (McGill University, Canada) for providing the SCO1 cells. SK acknowledges the University of Manitoba for seed funding through the University Research Grant Program (URGP). The Natural Sciences and Engineering Research Council of Canada (RGPIN-2019-05365) is acknowledged for its financial support.

## References

1. A. Timón-Gómez, *et al.*, Mitochondrial cytochrome c oxidase biogenesis: Recent developments. *Semin Cell Dev Biol* **76**, 163–178 (2018).
2. D. L. Nelson, M. M. Cox, “Oxidative Phosphorylation and Photophosphorylation” in *Lehninger Principles of Biochemistry*, Fourth, (W. H. Freeman, 2004), pp. 690–750.
3. Y. C. Horng, P. A. Cobine, A. B. Maxfield, H. S. Carr, D. R. Winge, Specific copper transfer from the Cox17 metallochaperone to both Sco1 and Cox11 in the assembly of yeast cytochrome c oxidase. *Journal of Biological Chemistry* **279**, 35334–35340 (2004).
4. M. Brischiari, M. Zeviani, Cytochrome c oxidase deficiency. *Biochimica et Biophysica Acta (BBA) - Bioenergetics* **1862**, 148335 (2021).
5. D. C. Wallace, Mitochondrial defects in cardiomyopathy and neuromuscular disease. *Am Heart J* **139**, 570–585 (2000).
6. F. Fontanesi, A. Barrientos, “Mitochondrial Cytochrome c Oxidase Assembly in Health and Human Diseases” in *Mitochondrial Disorders Caused by Nuclear Genes*, L.-J. C. Wong, Ed. (Springer New York, 2013), pp. 239–259.
7. I. Valnot, *et al.*, Mutations of the SCO1 gene in mitochondrial cytochrome c oxidase deficiency with neonatal-onset hepatic failure and encephalopathy. *Am J Hum Genet* **67**, 1104–1109 (2000).
8. J. C. von Kleist-Retzow, *et al.*, A High Rate ( 20%– 30%) of Parental Consanguinity in Cytochrome- Oxidase Deficiency. *Am J Hum Genet* **63**, 428–435 (1998).
9. G. S. Gorman, *et al.*, Prevalence of nuclear and mitochondrial DNA mutations related to adult mitochondrial disease. *Ann Neurol* **77**, 753–759 (2015).
10. E. A. Shoubridge, Cytochrome c oxidase deficiency. *Am J Med Genet* **106**, 46–52 (2001).

11. L. Stiburek, K. Vesela, H. Hansikova, H. Hulkova, J. Zeman, Loss of function of Sco1 and its interaction with cytochrome c oxidase. *Am J Physiol Cell Physiol* **296**, 1218–1226 (2009).
12. S. C. Leary, *et al.*, Human SCO1 and SCO2 have independent, cooperative functions in copper delivery to cytochrome c oxidase. *Hum Mol Genet* **13**, 1839–1848 (2004).
13. E. A. Shoubridge, Cytochrome c oxidase deficiency. *Am J Med Genet* **106**, 46–52 (2001).
14. P. Chakraborty, A. Feigenbaum, B. Robinson, “Photo\_Human Cytochrome Oxidase Deficiency” in *NORD Guide to Rare Disorders*, (Lippincott Williams & Wilkins, 2003), p. 895.
15. S. Parikh, *et al.*, Diagnosis and management of mitochondrial disease: a consensus statement from the Mitochondrial Medicine Society. *Genetics in Medicine* **17**, 689–701 (2015).
16. A. E. Frazier, D. R. Thorburn, Biochemical Analyses of the Electron Transport Chain Complexes by Spectrophotometry. *Methods in Molecular Biology* **837**, 49–62 (2012).
17. M. L. Simard, A. Mourier, L. C. Greaves, R. W. Taylor, J. B. Stewart, A novel histochemistry assay to assess and quantify focal cytochrome c oxidase deficiency. *Journal of Pathology* **245**, 311–323 (2018).
18. S. B. Wortmann, J. A. Mayr, J. M. Nuoffer, H. Prokisch, W. Sperl, A Guideline for the Diagnosis of Pediatric Mitochondrial Disease: The Value of Muscle and Skin Biopsies in the Genetics Era. *Neuropediatrics* **48**, 309–314 (2017).
19. J. L. Murphy, *et al.*, Cytochrome c oxidase-intermediate fibres: Importance in understanding the pathogenesis and treatment of mitochondrial myopathy. *Neuromuscular Disorders* **22**, 690–698 (2012).
20. A. Grünewald, *et al.*, Quantitative quadruple-label immunofluorescence of mitochondrial and cytoplasmic proteins in single neurons from human midbrain tissue. *J Neurosci Methods* **232**, 143–149 (2014).
21. J. M. Ross, Visualization of mitochondrial respiratory function using cytochrome C oxidase/succinate dehydrogenase (COX/SDH) double-labeling histochemistry. *Journal of Visualized Experiments*, 1–6 (2011).
22. D. Polcari, P. Dauphin-Ducharme, J. Mauzeroll, Scanning Electrochemical Microscopy: A Comprehensive Review of Experimental Parameters from 1989 to 2015. *Chem Rev* **116**, 13234–13278 (2016).
23. F. P. Filice, Z. Ding, Analysing single live cells by scanning electrochemical microscopy. *Analyst* **144**, 738–752 (2019).

24. I. Beaulieu, S. Kuss, J. Mauzeroll, M. Geissler, Biological scanning electrochemical microscopy and its application to live cell studies. *Anal Chem* **83**, 1485–1492 (2011).
25. S. Kuss, D. Polcari, M. Geissler, D. Brassard, J. Mauzeroll, Assessment of multidrug resistance on cell coculture patterns using scanning electrochemical microscopy. *Proceedings of the National Academy of Sciences* **110**, 9249–9254 (2013).
26. S. Kuss, D. Trinh, J. Mauzeroll, High-Speed Scanning Electrochemical Microscopy Method for Substrate Kinetic Determination: Application to Live Cell Imaging in Human Cancer. *Anal Chem* **87**, 8102–8106 (2015).
27. S. Darvishi, *et al.*, Tape-Stripping Electrochemical Detection of Melanoma. *Anal Chem* **91**, 12900–12908 (2019).
28. J. L. Connell, J. Kim, J. B. Shear, A. J. Bard, M. Whiteley, Real-time monitoring of quorum sensing in 3D-printed bacterial aggregates using scanning electrochemical microscopy. *Proc Natl Acad Sci U S A* **111**, 18255–18260 (2014).
29. N. M. Jayathilake, D. Koley, Glucose Microsensor with Covalently Immobilized Glucose Oxidase for Probing Bacterial Glucose Uptake by Scanning Electrochemical Microscopy. *Anal Chem* **92**, 3589–3597 (2020).
30. Y. Zhou, J. Zhang, Y. Zhao, Y. Liu, F. Li, Bacterial Biofilm Probed by Scanning Electrochemical Microscopy: A Review. *ChemElectroChem* **9** (2022).
31. N. Thomas, V. Singh, N. Ahmed, D. Trinh, S. Kuss, Single-cell scanning photoelectrochemical microscopy using micro-optical-ring electrodes. *Biosens Bioelectron* **217** (2022).
32. X. Zhao, R. Zhu, M. Anikovskiy, Q. Wu, Z. Ding, Profiling H<sub>2</sub>O<sub>2</sub> from single COS-7 cells by means of scanning electrochemical microscopy. *Biosens Bioelectron* **227** (2023).
33. K. Salvador-Severo, *et al.*, Mitochondrial proteomic profile of complex IV deficiency fibroblasts: rearrangement of oxidative phosphorylation complex/supercomplex and other metabolic pathways. *Bol Med Hosp Infant Mex* **74**, 175–180 (2017).
34. S. Bascomb, “Enzyme Tests in Bacterial Identification” in *Methods in Microbiology*, 19th Ed., R. R. Colwell, R. Grigorova, Eds. (Academic Press, 1988), pp. 105–160.
35. P. Jurtshuk, O. M. Marcucci, D. N. McQuitty, Tetramethyl-p-phenylenediamine oxidase reaction in *Azotobacter vinelandii*. *Appl Microbiol* **30**, 951–958 (1975).
36. S. Kuss, E. E. L. Tanner, M. Ordovas-Montanes, R. G. Compton, Electrochemical recognition and quantification of cytochrome c expression in *Bacillus subtilis* and aerobic/anaerobic *Escherichia coli* using N, N, N', N'-tetramethyl-para-phenylene-diamine (TMPD). *Chem Sci* **8**, 7682–7688 (2017).

37. A. J. Bard, F.-R. F. Fan, J. Kwak, O. Lev, Scanning Electrochemical Microscopy. Introduction and Principles. *Anal Chem* **61**, 132–138 (1989).
38. S. Kuss, D. Trinh, L. Danis, J. Mauzeroll, High-Speed Scanning Electrochemical Microscopy Method for Substrate Kinetic Determination: Method and Theory. *Anal Chem* **87** (2015).
39. G. Villani, G. Attardi, In vivo control of respiration by cytochrome c oxidase in wild-type and mitochondrial DNA mutation-carrying human cells. *Proc Natl Acad Sci U S A* **94**, 1166–1171 (1997).
40. D. G. Nicholls, S. J. Ferguson, “Respiratory Chains” in *Bioenergetics*, 4th Ed., (Academic Press, 2013), pp. 91–158.
41. J. K. Salabei, A. A. Gibb, B. G. Hill, Comprehensive measurement of respiratory activity in permeabilized cells using extracellular flux analysis. **9**, 421–438 (2014).
42. D. A. C. Brownson, C. E. Banks, *The Handbook of Graphene Electrochemistry* (2014) <https://doi.org/10.1007/978-1-4471-6428-9>.
43. S. Kuss, *et al.*, Assessing multidrug resistance protein 1-mediated function in cancer cell multidrug resistance by scanning electrochemical microscopy and flow cytometry. *Bioelectrochemistry* **82**, 29–37 (2011).
44. E. L. Bell, *et al.*, The Qo site of the mitochondrial complex III is required for the transduction of hypoxic signaling via reactive oxygen species production. *Journal of Cell Biology* **177**, 1029–1036 (2007).
45. S. Kuss, C. Kuss, D. Trinh, S. B. Schougaard, J. Mauzeroll, Forced convection during scanning electrochemical microscopy imaging over living cells: Effect of topographies and kinetics on the microelectrode current. *Electrochim Acta* **110**, 42–48 (2013).
46. I. Vercellino, L. A. Sazanov, The assembly, regulation and function of the mitochondrial respiratory chain. *Nat Rev Mol Cell Biol* **23**, 141–161 (2022).
47. P. Brzezinski, A. Moe, P. Adelroth, Structure and Mechanism of Respiratory III-IV Supercomplexes in Bioenergetic Membranes. *Chem Rev* **121**, 9644–9673 (2021).
48. P. Klement, L. G. J. Nijtmans, C. Van Den Bogert, J. Houštěk, Analysis of Oxidative Phosphorylation Complexes in Cultured Human Fibroblasts and Amniocytes by Blue-Native-Electrophoresis Using Mitoplasts Isolated with the Help of Digitonin. *Anal Biochem* **231**, 218–224 (1995).
49. H. Schägger, [12] Native electrophoresis for isolation of mitochondrial oxidative phosphorylation protein complexes. *Methods Enzymol* **260**, 190–202 (1995).
50. E. P. Booy, *et al.*, The RNA helicase RHAU (DHX36) unwinds a G4-quadruplex in human telomerase RNA and promotes the formation of the P1 helix template boundary. *Nucleic Acids Res* **40**, 4110–4124 (2012).

51. W. Strober, Trypan Blue Exclusion Test of Cell Viability. *Curr Protoc Immunol* **111**, A3.B.1-A3.B.3 (2015).